



OPEN ACCESS

EDITED BY Xiaobo Wang, Sun Yat-sen University, China

REVIEWED BY Keyan Chen, China Medical University, China Wei Zhang, Sun Yat-sen University, China

*CORRESPONDENCE Boyin Jia, i jiaboyin@jlau.edu.cn

i j Rui Du, □ duruijlau@163.com

RECEIVED 01 August 2025 ACCEPTED 10 September 2025 PUBLISHED 25 September 2025

Han X, Li X, Yan X, Zhang Y, Liu C, Liu W, Han R, Li Y, Li J, Diao N, Jia B and Du R (2025) 3D-ASC-Exos as a novel drug carrier for glioma treatment. Front. Cell Dev. Biol. 13:1677555. doi: 10.3389/fcell.2025.1677555

© 2025 Han, Li, Yan, Zhang, Liu, Liu, Han, Li, Li, Diao, Jia and Du. This is an open-access article distributed under the terms of the Creative Commons Attribution License (CC BY). The use, distribution or reproduction in other forums is permitted, provided the original author(s) and the copyright owner(s) are credited and that the original publication in this journal is cited, in accordance with accepted academic practice. No use, distribution or reproduction is permitted which does not comply with these terms.

3D-ASC-Exos as a novel drug carrier for glioma treatment

Xintong Han¹, Xin Li², Xinrui Yan², Yu Zhang², Chang Liu², Wei Liu², Rui Han², Yaxin Li², Jianming Li³, Naichao Diao³, Boyin Jia^{1,2,3}* and Rui Du^{1,3}*

¹College of Agriculture, Yanbian University, Yanji, China, ²College of Animal Science and Technology, Jilin Agricultural University, Changchun, China, ³Jilin Province Sika Deer Efficient Breeding and Product Development Technology Engineering Research Center, Jilin Agricultural University, Changchun, China

Introduction: It is known that extracts from deer antler stem cells have an inhibitory effect on glioma growth. Therefore, it is hypothesized that exosomes derived from deer antler stem cells (ASC-Exos) can be used as a new drug carrier for the treatment of glioma.

Methods: To begin with, we established a 3D culture system to obtain more exosomes and characterized the 3D-ASC-Exos. Subsequently, we loaded TMZ into 3D-ASC-Exos. Evaluate the effects of 3D-ASC-Exos loaded with TMZ on glioma cell proliferation, migration, invasion, and apoptosis at the cellular level. Additionally, the safety and efficacy of 3D-ASC-Exos loaded with TMZ against glioma were evaluated using tumor-bearing mice.

Results: Compared with the 2D-ASC-Exos obtained from the traditional 2D culture, the 3D-ASC-Exos obtained from our constructed 3D culture system were concentrated nearly 30 times in the culture medium volume, which was more convenient for subsequent puriffcation. The two forms of ASC-Exos had similar morphologies and surface markers, but 3D-ASC-Exos were enriched with more miRNAs related to tumor suppression. In vitro experiments demonstrated that 3D-ASC-exosomes loaded with temozolomide (TMZ) inhibited the proliferation, migration and invasion abilities of glioma cells and promoted the apoptosis of glioma cells. The vivo tumor-bearing mouse model demonstrated that 3D-ASC-Exos loaded with TMZ exerted tumorsuppressive effects by inhibiting tumor growth and promoting tumor apoptosis. Meanwhile, the treatment with 3D-ASC-Exos loaded with TMZ caused no damage to the various tissues and organs of mice compared with the TMZ group. Discussion: 3D-ASC-Exos can be used as a novel drug carrier for glioma treatment. The development of 3D-ASC-Exos as a drug carrier not only provides a better strategy for tumor treatment, but also demonstrates the broad potential of exosomes in targeted tumor therapy.

KEYWORDS

antler, 3D-ASC-Exos, glioma, drug carrier, TMZ

1 Introduction

Exosomes are nano-sized vesicular structures secreted by cells, and they contain bioactive molecules such as proteins, RNA, and DNA inside (van Niel et al., 2022). An increasing number of studies show that exosomes derived from different mesenchymal stem cells (MSCs), such as bone marrow mesenchymal stem cells (BMSCs), adipose mesenchymal

stem cells (AMSCs) and human umbilical cord mesenchymal stem cells (hUCMSCs) play significant roles in inhibiting the progression of breast cancer, colon cancer and bladder cancer, respectively (Safari et al., 2023; Zhang et al., 2020; Wu et al., 2013). In addition, the anticancer ability of MSCs-derived exosomes as drug carriers has been confirmed in many studies. Compared with simple drug treatment, the therapeutic effect of exosome-loaded drugs was better, and it reduced the adverse effects on the body caused by the intake of pure drugs (Hu et al., 2022). Therefore, MSCs-derived exosomes have emerged as an ideal carrier for drug delivery. However, the latest research has found that MSCs have pro-cancer effects such as promoting tumor angiogenesis, reshaping the immunosuppressive microenvironment, and transmitting oncogenic miRNAs through exosomes (Guo et al., 2020; Liang et al., 2021). Therefore, it is necessary to seek safer stem cell resources.

Antler is the only mammalian organ that can regenerate periodically (Nieto-Diaz et al., 2012). Antler regeneration is a process based on antler stem cells (ASCs). Antler regeneration consumes approximately 3.3 million ASCs each year. In less than 60 days, antler weighing 10 kg is formed (Li et al., 2023). The growth rate of antler is 30 times that of tumors. But antler and its surrounding tissues do not undergo cancerous transformation (Jia et al., 2021). Therefore, ASCs have a strong resistance to tumors. ASCs preferentially migrate towards tumors and regulate the progression of tumor cells through paracrine rather than cellular means. Among them, ASC-Exos play a major role in paracrine secretion (Liu et al., 2023). Glioma is a common type of malignant brain tumor (Fernandes et al., 2017). The current common treatment approach is surgical resection, supplemented by temozolomide (TMZ) for radiotherapy and chemotherapy (Jezierzański et al., 2024). However, due to primary or acquired drug resistance mechanisms, the efficacy of TMZ is limited. Compared with TMZ, the extract from the tip of antler exerts anti-glioma effects by cell cycle arrest, and has no toxicity to non-cancer cells (Chonco et al., 2021). Therefore, we speculate that ASC-Exos can be used as nanodrugs or drug delivery carriers for the treatment of glioma.

At present, the relatively mature MSCs culture process in clinical practice is the 2D culture mode. This mode, due to high production costs and cumbersome operations, cannot meet the demands of large-scale production. In recent years, an increasing number of research reports have indicated that 3D culture mode is more similar to the microenvironment within the body. The 3D culture mode can obtain higher-quality exosomes by controlling the parameters (such as temperature, pH, etc.) during the cell growth process, while maintaining the surface characteristics of the exosomes (Phan et al., 2018). In addition, the exosome population obtained in the 3D culture system is more diverse and freer from serum protein contamination (Storm et al., 2016; Gobin et al., 2021; Yan et al., 2018). However, reports on the optimization of 3D culture systems for ASCs are still quite limited. In this study, we employed a 3D culture system to produce high-quality and high-concentration 3D-ASC-Exos. And investigate the effects of 3D-ASC-Exos loaded with drugs (TMZ) in vitro on the proliferation, migration, invasion and apoptosis of glioma cells. Subsequently, we further evaluated the therapeutic effect and safety of 3D-ASC-Exos loaded with drugs (temozolomide) on tumor-bearing mice. In conclusion, 3D-ASC-Exos efficiently prepared through the 3D culture system can be used as drug delivery carriers to treat glioma.

2 Materials and methods

2.1 Isolation and identification of ASCs

Collagenase I (64 mg), collagenase II (52 mg), and collagenase IV (44 mg) were dissolved together in 80 mL of DMEM and then filtered through a 0.22-micron membrane to prepare the tissue digestion enzyme for later use. We isolated the translucent mesenchymal layer from the tip of the antler. After digestion in a tissue digestion mixed enzyme, it was used for primary cell culture. We identified the cell morphology, trilineage differentiation ability and surface markers of the third-generation ASCs.

2.2 Cultivation of ASCs in 3D culture systems

Fetal bovine serum was centrifuged at 4 °C, 160,000×g, and 16 h. Collect the clear liquid on the top layer after centrifuging the fetal bovine serum, and this liquid is the low exosome serum. The inner diameter of the fibers in the medium-sized hollow fiber bioreactor was approximately 200 µm. The fibrous material was composed of polysulfone (PS) and polyvinylidene fluoride (PVDF). Each culture tube could hold approximately 20 mL of culture medium. The 3D culture system was successively circulated internally and externally with enzyme-free and sterile PBS, DMEM, and complete medium containing 10% fetal bovine serum for 24-48 h. Then, the ASCs were inoculated into the outer circulation culture cylinder of the 3D system and repeatedly tapped until the cells adhered evenly. We would invert the culture tube up and down every 30 min, and then connect it to the complete culture medium after 2 h and 30 min. The sugar consumption in the complete culture medium should be checked every other day to replace it with fresh complete culture medium in a timely manner.

2.3 Isolation and identification of 3D-ASC-Exos

Firstly, ELISA and PCR were respectively used to detect the contents of *Chlamydia* and *Mycoplasma* in the supernatants of 2D-ASCs and 3D-ASCs. Then, the supernatant was subjected to gradient centrifugation to harvest exosomes. Briefly, the process involved centrifugation at 4 °C for 15 min at 300×g, followed by 30 min at 2000×g, then 30 min at 10,000×g, and finally 2 h at 120,000×g. Finally, 2D-ASC-Exos and 3D-ASC-Exos were identified by transmission electron microscopy, nanoparticle tracking, and WB.

2.4 Small RNA sequencing of 3D-ASC-Exos

Firstly, we used the exoRNeasy Maxi kit to purify the RNA of 2D-ASC-Exos and 3D-ASC-Exos. Secondly, the qualified 2D-ASC-Exos and 3D-ASC-Exos were subjected to library construction using the Small RNA Sample Pre Kit. Finally, the obtained data were subjected to sRNA length screening, reference sequence alignment analysis, known miRNAs analysis, repeat sequence alignment, miRNAs differential expression analysis, and GO/KEGG enrichment analysis

of candidate target genes. The raw transcriptome data from this study have been submitted to the NCBI Gene Expression Omnibus with accession number GSE305022 (https://www.ncbi.nlm.nih.gov/geo/query/acc.cgi?acc=GSE305022).

2.5 *In vitro* evaluation of the effect of 3D-ASC-Exos loaded with TMZ on inhibiting glioma cells

After labeling TMZ with fluorescein isothiocyanate (FITC), 3D-ASC-Exos (100 μg/mL) were co-incubated with TMZ (10 μg/mL) at room temperature for 18 h. The 3D-ASC-Exos loaded with TMZ were separated from the supernatant by ultracentrifugation. The fluorescence intensity in the supernatant before and after centrifugation was detected to determine the loading amount. The 3D-ASC-Exos loaded with TMZ were placed in dialysis bags, and the percentage of drug release in the solution outside the dialysis bags was detected at 0 h, 4 h, 8 h, 12 h, 16 h, 20 h and 24 h respectively. 3D-ASC-Exos (100 μg/mL) and the positive drug TMZ (10 μg/mL) were used as controls. CCK8 was used to evaluate the proliferation ability of U87 and A172. At the same magnification as the original image (200X), the quantitative method for scratches was to divide the width of the scratch by the total width of the image. Cell scratch and Transwell were used to evaluate the migration levels of U87 and A172. Transwell was used to evaluate the invasive ability of U87 and A172(In addition to the materials used in the migration assay, Matrigel was also used). TUNEL was used to evaluate the apoptosis levels of U87 and A172. Q-PCR and WB were used to detect the expression of BAX, BCL2, P53 and EGFR in U87 and A172.

2.6 *In vivo* evaluation of the safety and efficacy of 3D-ASC-Exos loaded with TMZ in anti-glioma treatment

All experimental procedures involving animals were conducted in accordance with the ethical policies and guidelines approved by the Animal Ethics Committee of Jilin Agricultural University (Approval no. 20230315010). Due to technical limitations, in situ tumor modeling was not used to treat tumor-bearing mice in this experiment. Established a U87 tumor-bearing mouse model. Twelve female BALB/c nude mice were randomly selected. Dilute 5×10^6 U87 cells in 0.15 mL PBS. Then, inoculate them subcutaneously 0.5 cm lateral to the right thigh. One week later, the tumorbearing nude mice were treated. The samples were divided into the following four groups: 3D-ASC-Exos group (100 µg/mL), TMZ group (10 µg/mL), 3D-ASC-Exos + TMZ group (100 µg/mL), and Control group (PBS). Treat once every other day for 20 consecutive days. During the treatment period, the body weight and tumor size of the nude mice were measured every other day, and the measurement curves were plotted. At the end of the experiment, the mice were anesthetized with chloral hydrate. The tumor was removed, photographed and weighed. Routine blood tests were used to evaluate physiological indicators. Blood biochemistry was used to assess liver and kidney functions. HE staining was used to evaluate the injury levels of the heart, liver, spleen, lung and kidney. HE staining was used to evaluate the cellular morphology and tissue structure of tumors. TUNEL staining was used to detect the level of apoptosis in tumors. Ki67 was used to detect the level of cell proliferation. Immunohistochemical detection was performed to examine the expression of BAX, BCL2, P53 and EGFR.

2.7 Analysis of data

We used the software SPSS to conduct statistical difference analysis on all the data. The analysis method of this experiment was one-way analysis of variance. GraphPad and Origin were used to plot the data. Statistical differences were indicated by P. Within a group, P < 0.05 was marked with "*", P < 0.01 with "**", and P < 0.001 with "**"

3 Results and discussion

3.1 Identification of ASCs

We successfully obtained primary ASCs by collagenase digestion (Figure 1A). The proliferation ability of ASCs cultured up to the third generation remained good, and their morphology was mostly long spindle-shaped (Figure 1B). The IFA results of ASCs showed that CD73 and CD90 were highly expressed, while CD45 and CD34 were not expressed (Figure 1C). This result ruled out the possibility of other types of cells being mixed in the obtained cells, further clarifying the purity and specificity of the isolated cells. The trilineage differentiation staining results of ASCs showed that ASCs successfully differentiated into adipocytes, osteocytes and chondrocytes, respectively (Figures 1D-F). Q-PCR results indicated that the three types of cells after induction differentiation expressed the marker genes of adipocytes, osteocytes and chondrocytes, respectively (Figure 1G). The above results indicate that the ASCs we isolated and extracted meet the identification criteria for MSCs set by the International Society for Stem Cell Research (Dominici et al., 2006). The multipotent differentiation potential of ASCs was closely related to their paracrine function, and as an important carrier of paracrine action, the functional activity of ASC-Exos may be associated with the biological characteristics of ASCs. We identified that the extracted ASCs were MSCs, and this result provided a solid cell biological foundation for the subsequent exploration of 3D-ASC-Exos as drug carriers in the treatment of glioma.

3.2 3D culture of ASCs and identification of 3D-ASC-Exos

Hollow fiber bioreactors are a type of bioreactor used for 3D cell culture and can also be employed to obtain high concentrations of exosomes. The hollow fiber cell culture bioreactor mimics the human physiological circulatory system, providing a growth environment for cells that is closer to that of a living body (Cao et al., 2020). The secretory products of 3D-cultured cells are 10–100 times that of 2D-cultured cells, making it the ideal method for culturing exosomes at present (Watson et al., 2016). So far, 3D culture technology has been applied to the cultivation of hUCMSCs, BMSC, AMSCs, etc. However, the experience in culturing ASCs is

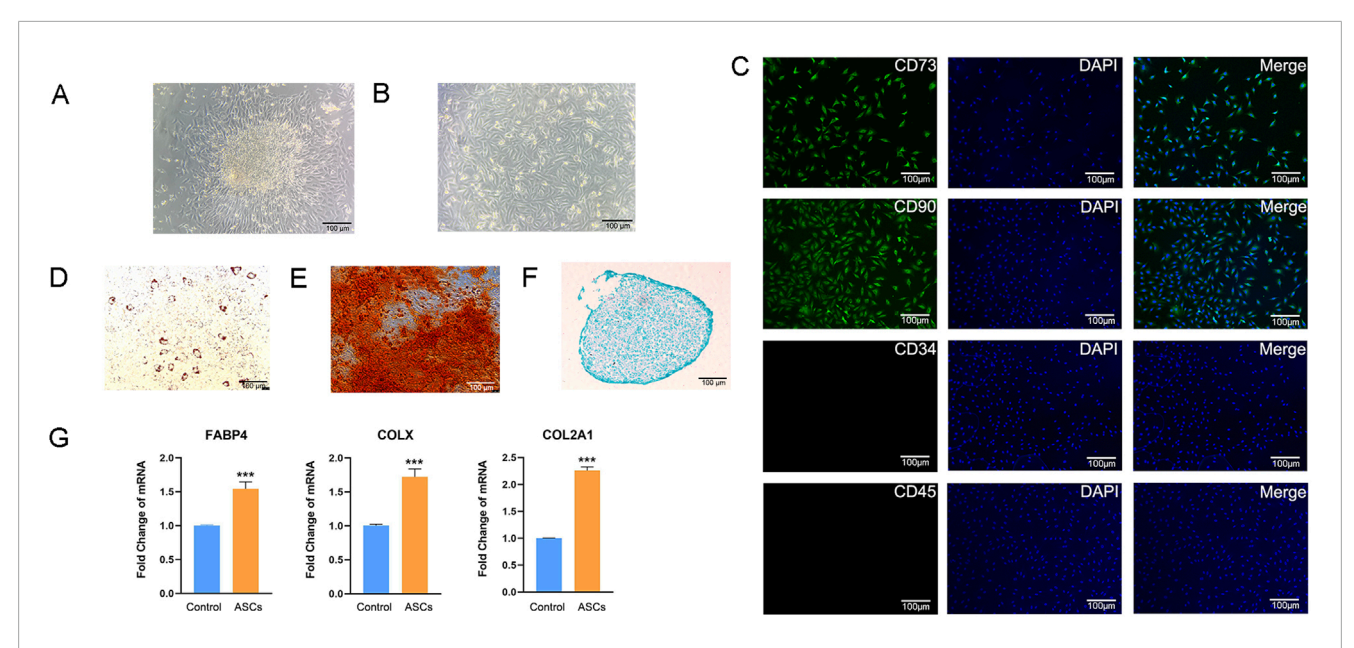


FIGURE 1 Isolation and identification of ASCs. (A) ASCs emigrated from tissues. (B) ASCs cultured to the third generation. (C) Immunofluorescence analysis of surface markers of ASCs. (D) Oil Red O staining of ASCs induced to adipogenic differentiation after 14 days. (E) Alizarin Red staining of ASCs induced to osteogenic differentiation after 14 days. (G) Q-PCR analysis of the expression levels of three marker genes after induction of differentiation (n = 3). Data were presented as mean \pm SD. One-way ANOVA combined with Tukey's HSD test and Bonferroni correction was used. P < 0.05,**P < 0.001.***P < 0.001.

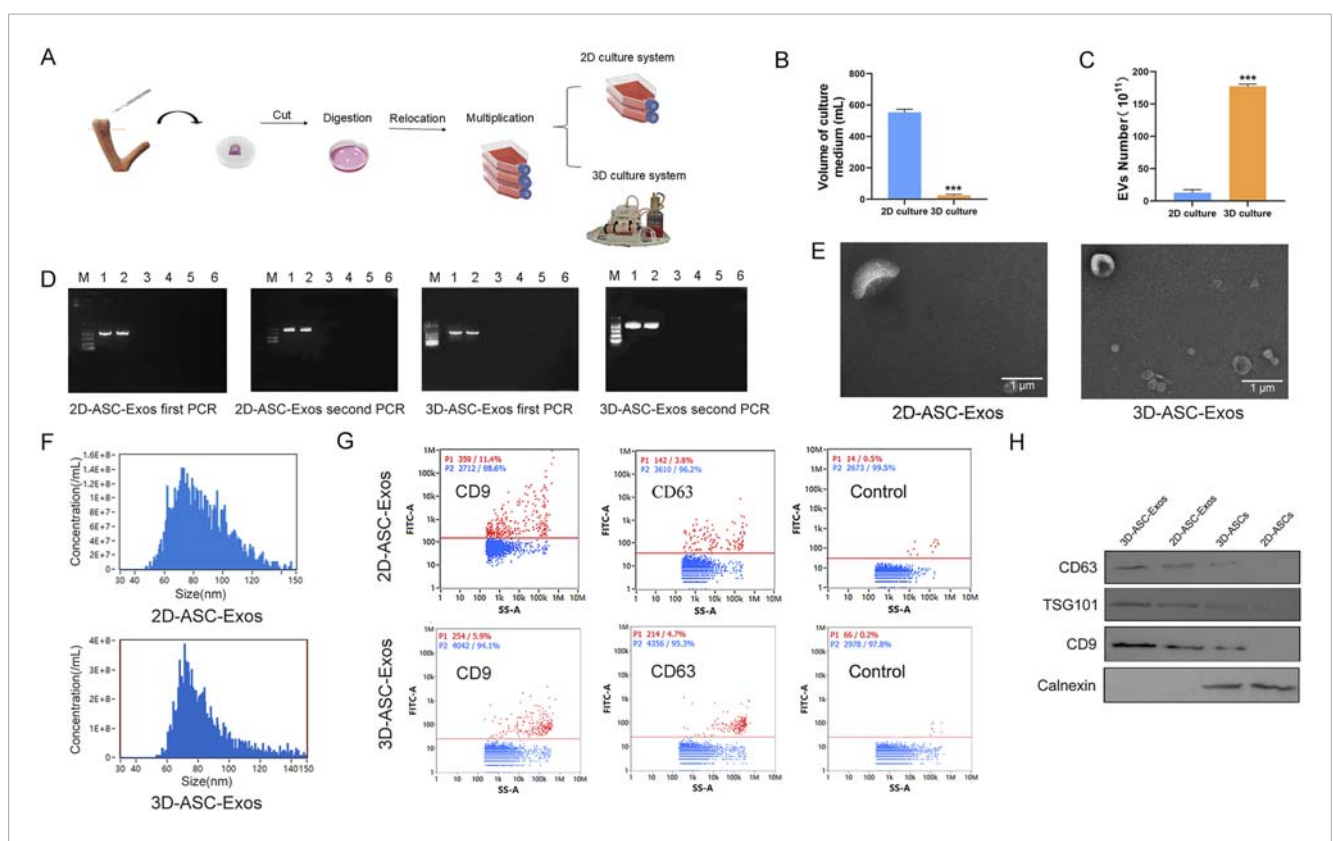
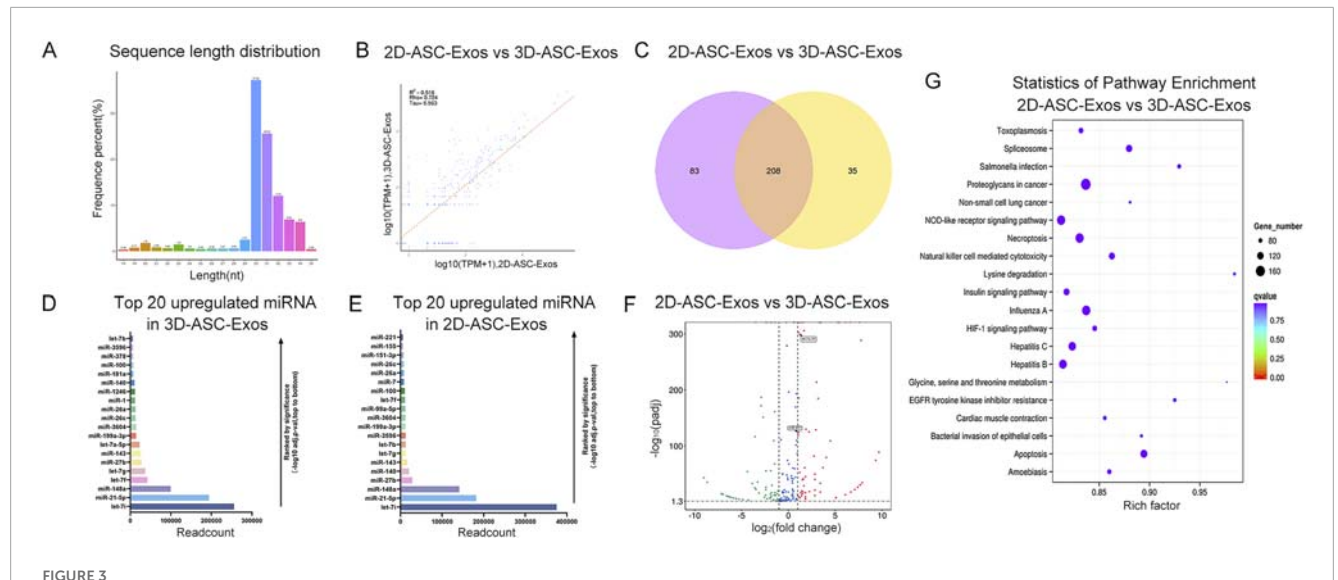


FIGURE 2 Isolation and identification of 3D-ASC-Exos. (A) Technical routes for 2D and 3D culture of ASCs. (B) Volume of culture medium used for the production of 4×10^{11} ASC-Exos (n = 3). (C) Number of exosomes produced per 10^8 ASCs. (D) ELISA detection of *Chlamydia* content in the supernatants of 2D-ASCs and 3D-ASCs. (E) Transmission electron microscopy images of the two types of ASC-Exos. (F) Nanoparticle tracking analysis of the diameter size distribution of the two types of ASC-Exos. (G) Nanoflow cytometry analysis of the expression of markers CD63 and CD9 on the two types of ASC-Exos. (H) WB analysis of the expression of markers CD63, TSG101, CD9 and Calnexin on the two types of ASC-Exos. Data were presented as mean \pm SD. One-way ANOVA combined with Tukey's HSD test and Bonferroni correction was used.*P < 0.05,**P < 0.01,***P < 0.001.



MiRNA expression profile analysis of 3D-ASC-Exos. (A) Length distribution of miRNAs in 3D-ASC-Exos. (B) Correlation analysis of 3D-ASC-Exos and 2D-ASC-Exos. (C) Venn diagram showing miRNAs of the two ASC-Exos. (D) TPM values of the top 20 highly expressed miRNAs in 3D-ASC-Exos. (E) TPM values of the top 20 highly expressed miRNAs in 2D-ASC-Exos. (F) Volcano plot showed differentially expressed miRNAs of the two ASC-Exos. (G) KEGG enrichment analysis of target genes of differentially expressed miRNAs. Data were presented as mean \pm SD. One-way ANOVA combined with Tukey's HSD test and Bonferroni correction was used.*P < 0.05,**P < 0.01,***P < 0.001.

still very limited (Lv et al., 2024; Wu et al., 2025; Ueyama et al., 2023). We established a 3D hollow fiber bioreactor system of ASCs (Figure 2A). We compared the difference in the number of exosomes harvested from 2D culture systems and 3D culture systems. The results indicated that when the same number of cells (approximately 1.2×10^7) were cultured, the total amount of exosomes collected at one time in the 3D culture system was basically the same as that in the 2D culture system. However, culturing these cells in a 2D system required 30 culture flasks each time, with each flask needing 15-20 mL of culture medium; while in a 3D system, only about 20 mL was needed. Therefore, the volume of culture medium required for 3D culture systems was nearly 30 times less than that for 2D culture systems. The results showed that when the number of ASCs was the same, the total amount of exosomes collected once from the 3D culture system was basically the same as that from the 2D culture system, but the volume of the culture medium was nearly 30 times less (Figure 2B). In addition, In the 2D culture system, the maximum harvest frequency of exosomes was 3-4 times, while in the 3D culture system it was 30 times (Figure 2C). In our research, compared with the 2D culture system, the 3D culture system had advantages such as a large yield, less consumables, and convenient operation, which could support subsequent largescale in vivo and in vitro experiments for the treatment of glioma. To identified the biological functions of ASC-Exos collected in a 3D environment. First, we respectively identified the supernatants harvested from the 2D culture system and the 3D culture system. The ELISA results of *Chlamydia* antibodies showed that the supernatants of both ASCs were negative (Attached Supplementary Table S1). The PCR results of Mycoplasma marker genes showed that the supernatants of both ASCs were negative (Figure 2D). The above results indicated that the supernatants harvested from both culture systems were free of Chlamydia and Mycoplasma contamination. Subsequently, we collected 2D-ASC-Exos and 3D-ASC-Exos by

gradient ultracentrifugation and identified them. The results of transmission electron microscopy observation showed that the two types of ASC-Exos were in the form of hollow vesicles and had a double-layer lipid membrane structure (Figure 2E). The results of nanoparticle tracking analysis showed that the average particle diameters of the two ASC-Exos were both around 75 nm, which was within the common range of exosome particle sizes (30–150 nm) (Figure 2F). After standard calibration, the sample concentrations of 2D-ASC-Exos and 3D-ASC-Exos were 5×10^8 and 1.77×10^{10} particles/mL, respectively. The protein contents of 2D-ASC-Exos and 3D-ASC-Exos determined by BCA were $2 \times 10^3 \,\mu\text{g/mL}$ and 6×10^4 µg/mL, respectively. This was equivalent to approximately $4 \times 10^{-6} \,\mu g$ and $3.39 \times 10^{-6} \,\mu g$ of protein for each 2D-ASC-Exos and 3D-ASC-Exos, respectively. Nanoflow cytometry results showed that both types of ASC-Exos expressed the exosome marker proteins CD9 and CD63 (Figure 2G). The WB results indicated that both ASC-Exos expressed exosome marker proteins CD63, CD9, TSG101 and Calnexin (Figure 2H). The above results indicated that, compared with 2D-ASC-Exos, the morphology and properties of 3D-ASC-Exos were normal. These findings lay a solid foundation for exploring the therapeutic potential of 3D-ASC-Exos as drug delivery carriers in cancer treatment.

3.3 MiRNA expression profiling of 3D-ASC-Exos

To evaluate the miRNAs expression profile of 3D-ASC-Exos, we performed Small RNA sequencing on them. And compared with our previous sequencing results of 2D-ASC-Exos. The results showed that the miRNAs of 3D-ASC-Exos were mainly distributed in the range of 30–32 nt in length, while those of 2D-ASC-Exos were mainly around 31 nt (Figure 3A). The sample correlation analysis

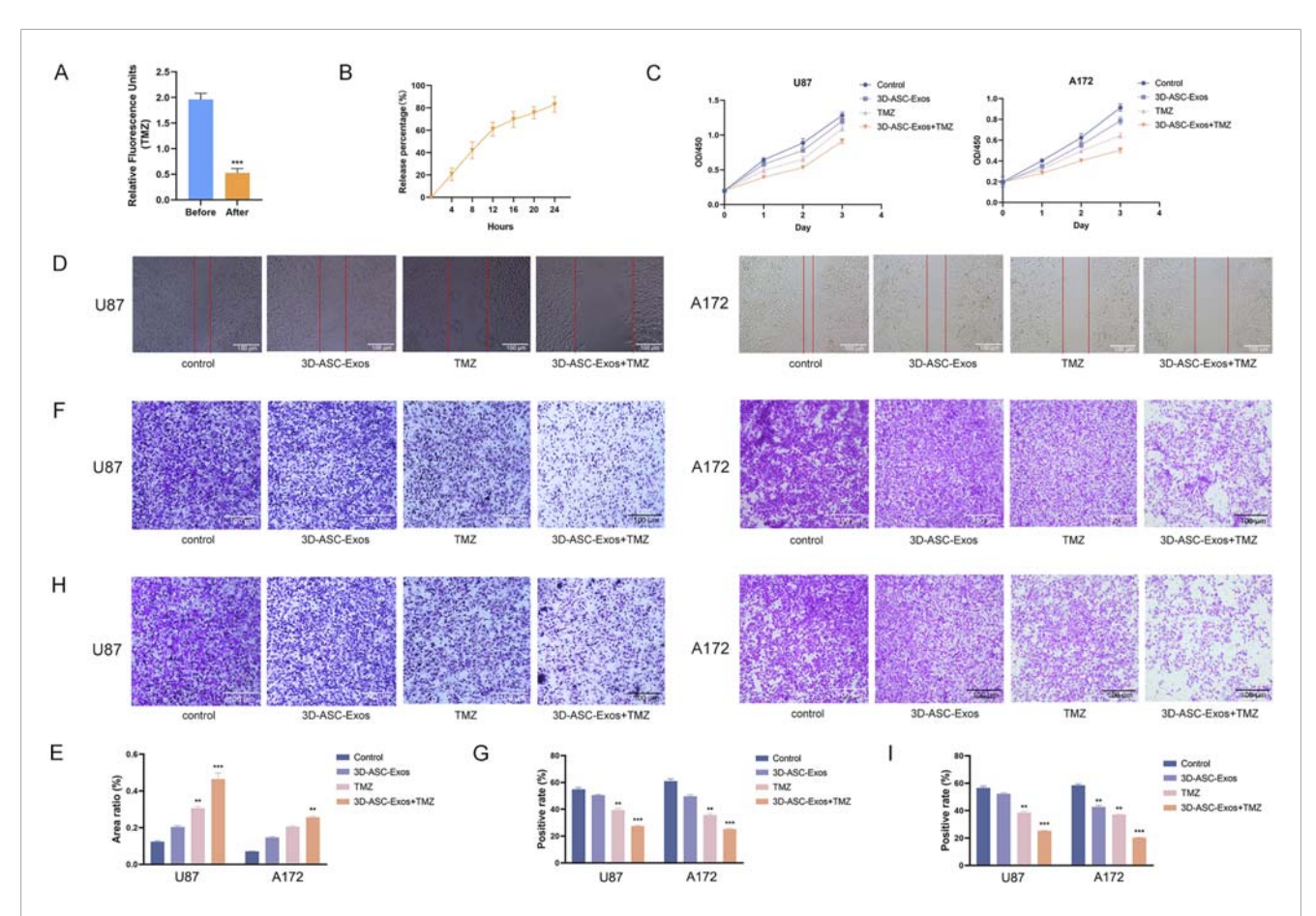
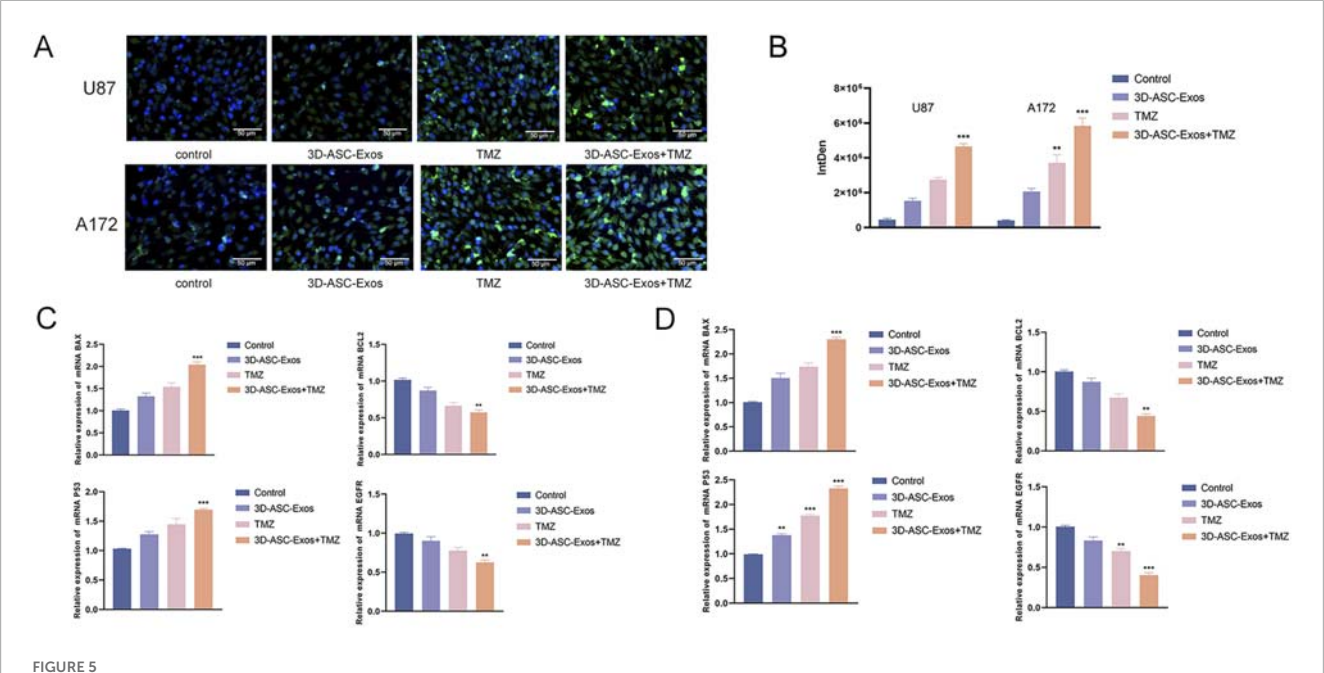


FIGURE 4
The effects of 3D-ASC-Exos loaded with TMZ on the proliferation, migration and invasion of glioma cells. (A) Relative fluorescence units of TMZ before and after ultracentrifugation (n = 3). (B) In vitro release profile of free TMZ in PBS for 24 h (n = 3). (C) CCK8 assay for the effect of 3D-ASC-Exos loaded with TMZ on the viability of U87 and A172 cells (n = 3). (C) CCK8 assay for the effect of 3D-ASC-Exos loaded with TMZ on the viability of U87 and A172 cells. (E) Quantitative analysis of the scratch area (n = 3). (F) Transwell assay for the effect of 3D-ASC-Exos loaded with TMZ on the migration ability of U87 and A172 cells. (G)
Quantitative analysis of the cell migration level (n = 3). (H) Transwell assay for the effect of 3D-ASC-Exos loaded with TMZ on the invasion ability of U87 and A172 cells. (I) Quantitative analysis of the cell invasion level (n = 3). Data were presented as mean ± SD. One-way ANOVA combined with Tukey's HSD test and Bonferroni correction was used.*P < 0.05,**P < 0.01,***P < 0.001.

results showed that the correlation coefficient was 0.516 (Figure 3B). The Venn diagram results showed that 208 miRNAs were common miRNAs of the two ASC-Exos (Figure 3C). Furthermore, among the top 20 highly expressed miRNAs of the two ASC-Exos, 15 miRNAs were consistent (Figures 3D,E). The results of differential miRNAs analysis showed that a total of 200 miRNAs were differentially expressed, among which 98 miRNAs were upregulated and 102 miRNAs were downregulated (Figure 3F). Among them, some upregulated miRNAs were closely related to the regulation of glioma cells. For instance, let-7a-5P has the function of inhibiting the proliferation of glioma and suppressing the stemness of glioma cells (Chen et al., 2022); miR-451 can inhibit the proliferation of glioma cells and also reduce the resistance of glioma cells to TMZ through the mTOR signaling pathway (Ogawa et al., 2019; Zhao et al., 2017). KEGG enrichment analysis was performed on the target genes of differentially expressed miRNAs (Figure 3G). Notably, the top 20 significantly different KEGG pathways were mostly related to tumor regulatory mechanisms such as uncontrolled proliferation, apoptosis resistance, immune escape, and metabolic reprogramming, including Proteoglycans in cancer, Non-small cell lung cancer, HIF-1 signaling pathway, Apoptosis, EGFR tyrosine kinase inhibitor resistance, Natural killer cell mediated cytotoxicity, Necroptosis, Spliceosome, NOD-like receptor signaling pathway, Glycine, serine and threonine metabolism (Kizhakkeppurath Kumaran et al., 2023; Mithoowani and Febbraro, 2022; Liu et al., 2021; Moyer et al., 2025; de Miguel et al., 2023; Bushnell et al., 2024; Zhou et al., 2023). Overall, compared with 2D-ASC-Exos, 3D-ASC-Exos were enriched with a higher proportion of miRNAs related to tumor regulation, suggesting that they have greater application potential in tumor treatment.

3.4 *In vitro* evaluation of the effects of 3D-ASC-Exos loaded with TMZ on the proliferation, migration, invasion and apoptosis of glioma cells

The fluorescence intensity comparison indicated that approximately 76.9% of TMZ was encapsulated in 3D-ASC-Exos

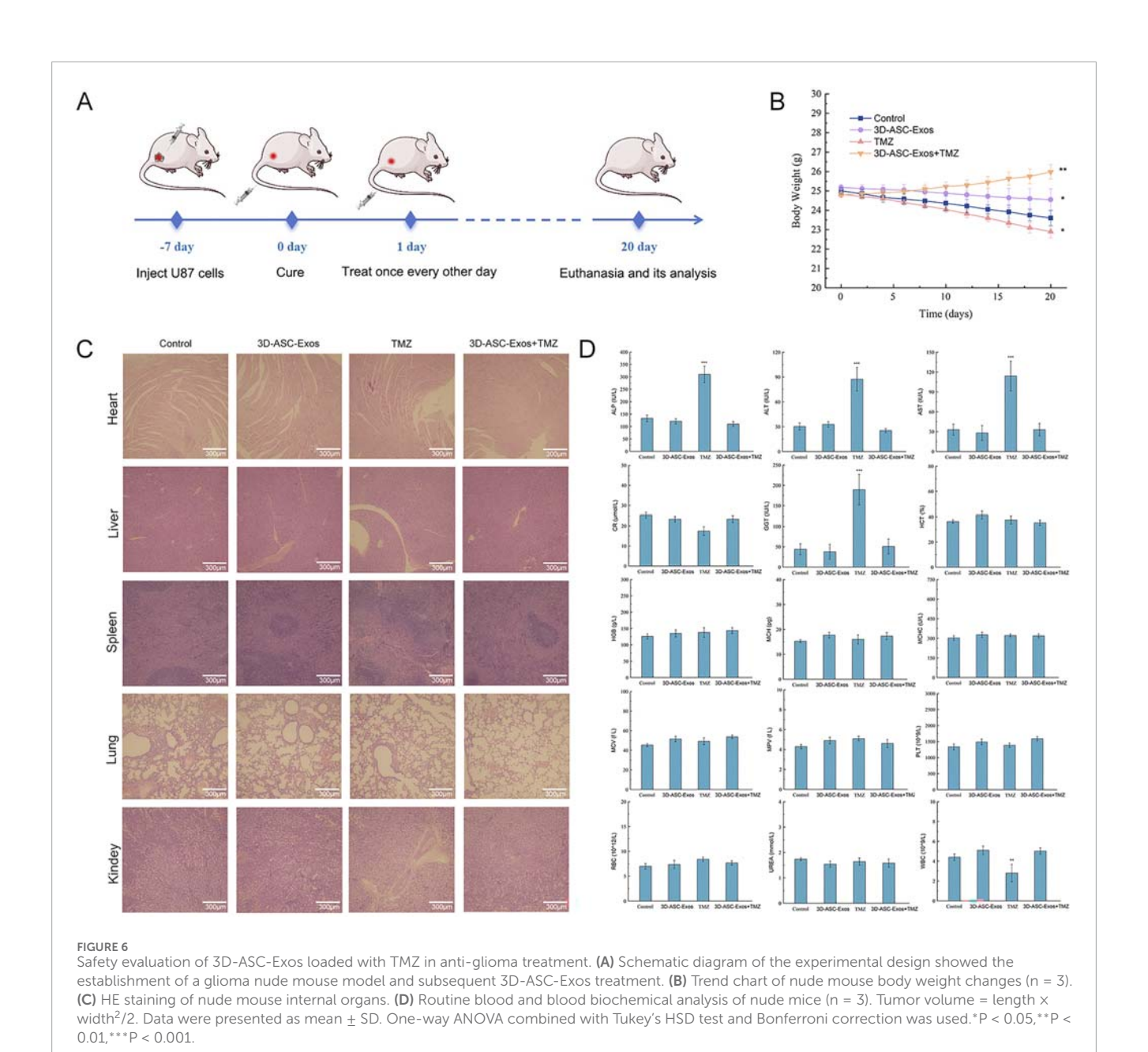


The effect of 3D-ASC-Exos loaded with TMZ on glioma cells. (A) TUNEL assay for the effect of 3D-ASC-Exos loaded with TMZ on the apoptosis ability of U87 and A172 cells. (B) Quantitative analysis of apoptosis levels (n = 3). (C) Q-PCR detection of the expression levels of BCL2, EGFR, P53, and BAX genes in U87 cells (n = 3). (D) Q-PCR detection of the expression levels of BCL2, EGFR, P53, and BAX genes in A172 cells (n = 3). The relative gene expression levels were calculated using the $2^{-\Delta\Delta Ct}$ method. Data were presented as mean \pm SD. One-way ANOVA combined with Tukey's HSD test and Bonferroni correction was used.*P < 0.05,**P < 0.01,***P < 0.001.

(Figure 4A). Moreover, the TMZ encapsulated in 3D-ASC-Exos could be gradually released into the external environment over time. By 24 h, approximately 83% of the TMZ had been released into the external environment (Figure 4B). We evaluated the effect of 3D-ASC-Exos loaded TMZ on inhibiting glioma in vitro. The CCK8 assay results indicated that the inhibitory effect of 3D-ASC-Exos loaded with TMZ on the proliferation ability of glioma cells was superior to that of using 3D-ASC-Exos or TMZ alone (Figure 4C). The cell scratch and Transwell results indicated that the inhibitory effect of 3D-ASC-Exos loaded with TMZ on the migration ability of glioma cells was superior to that of using 3D-ASC-Exos or TMZ alone, and the synergistic effect had more therapeutic advantages (Figures 4D-G). The Transwell assay results indicated that 3D-ASC-Exos loaded with TMZ significantly inhibited the invasion ability of glioma cells (Figures 4H,I). The TUNEL results showed that the 3D-ASC-Exos loaded with TMZ had the highest fluorescence intensity, indicating that it had the best effect in promoting glioma cell apoptosis (Figures 5A,B). The Q-PCR results indicated that 3D-ASC-Exos loaded with TMZ significantly inhibited the expression of the proto-oncogenes BCL2 and EGFR, and promoted the expression of the tumor suppressor genes P53 and BAX (Figures 5C,D). The above results indicated that 3D-ASC-Exos loaded with TMZ had the effects of inhibiting the proliferation, migration and invasion of glioma cells and promoting apoptosis. The application of exosomes as a nanocarrier system in tumor therapy had attracted extensive attention from scholars. Wei et al. found that compared with pure drug treatment, exosomes derived from MSCs carrying doxorubicin had a better inhibitory effect on the proliferation of osteosarcoma cells in vitro and were less toxic to the cells (Wei et al., 2019). Bagheri et al. found that exosomes derived from MSCs loaded with docetaxel could highly accumulate at tumor sites and significantly inhibit tumor growth. Meanwhile, compared with the sole use of docetaxel, the docetaxel-loaded exosomes derived from MSCs were metabolized by the liver at a faster rate (Bagheri et al., 2020). Despite a large number of studies confirmed that MSC-Exos, as drug carriers, possess numerous advantages in cancer treatment, they could efficiently inhibit tumor cell proliferation, promote tumor cell apoptosis, and enhance drug efficacy. However, in the complex physiological and pathological environment, the functions of MSC-Exos were not constant. In recent years, there have been reports that exosomes derived from MSCs can also exhibit promoting effects on cancer cells. Zhao et al. discovered that exosomes derived from BMSCs promoted the proliferation and migration of and osteosarcoma cells, as well as tumor occurrence (Zhao et al., 2019). Ren et al. found that BMSC-Exos pretreated with hypoxia inhibited the expression levels of pro-apoptotic genes (such as PTEN, PDCD4 and RECK) through miR-21-5p, thereby slowing down the apoptosis process of lung cancer cells (Ren et al., 2019). Therefore, it is necessary for us to find more exosomes derived from mesenchymal stem cells for tumor treatment. ASCs were the basis for the rapid growth of antler without causing cancer. As a novel type of MSCs, ASCs had demonstrated significant advantages in targeted glioma therapy due to their inherent anti-glioma properties and load-bearing plasticity.

3.5 *In vivo* evaluation of the safety and efficacy of 3D-ASC-Exos loaded with TMZ in anti-glioma therapy

An increasing amount of clinical evidence indicated that exosomes could not only enhance the therapeutic effect of drugs



but also reduce the systemic toxicity of chemotherapy drugs (Liang et al., 2021). To evaluate the safety of 3D-ASC-Exos loaded TMZ *in vivo* against glioma, 3D-ASC-Exos were used to treat U87 glioma nude mice (Figure 6A). On the seventh day after subcutaneous injection of U87 cells in nude mice, PBS, 3D-ASC-Exos (500 µg/mL), TMZ (50 µg/mL), and 3D-ASC-Exos + TMZ (500 µg/mL) were respectively administered via tail vein injection of 0.1 mL every other day. During the 20-day treatment period, the body weight of nude mice in the 3D-ASC-Exos + TMZ group not only did not decrease but also showed a slight upward trend (Figure 6B). The results of HE staining of the internal organs of mice showed that 3D-ASC-Exos loaded with TMZ had no damage to the heart, liver, spleen, lung and kidney of mice after treatment (Figure 6C). Routine blood tests and blood biochemical analyses revealed that the levels of ALP, ALT, AST, and GGT in the TMZ

group significantly increased, while the WBC count decreased. However, the values of each group in the 3D-ASC-Exos + TMZ group and the 3D-ASC-Exos group showed no difference from those in the Control group (Figure 6D). The results indicated that the treatment method of 3D-ASC-Exos loaded with TMZ had no effect on the physiological indicators and liver-kidney functions of nude mice with glioma. The above results suggested that 3D-ASC-Exos had good systemic safety and biocompatibility. In addition, 3D-ASC-Exos loaded with TMZ in the treatment of glioma-bearing nude mice reduced the damage of chemotherapy drugs to the body. We further evaluated the *in vivo* anti-glioma effect of 3D-ASC-Exos loaded with TMZ. Overall observation results indicated that the tumors in the 3D-ASC-Exos + TMZ group were significantly smaller than those in the TMZ group (Figures 7A,B). Even the tumor of one of them had disappeared, indicating that the tumor

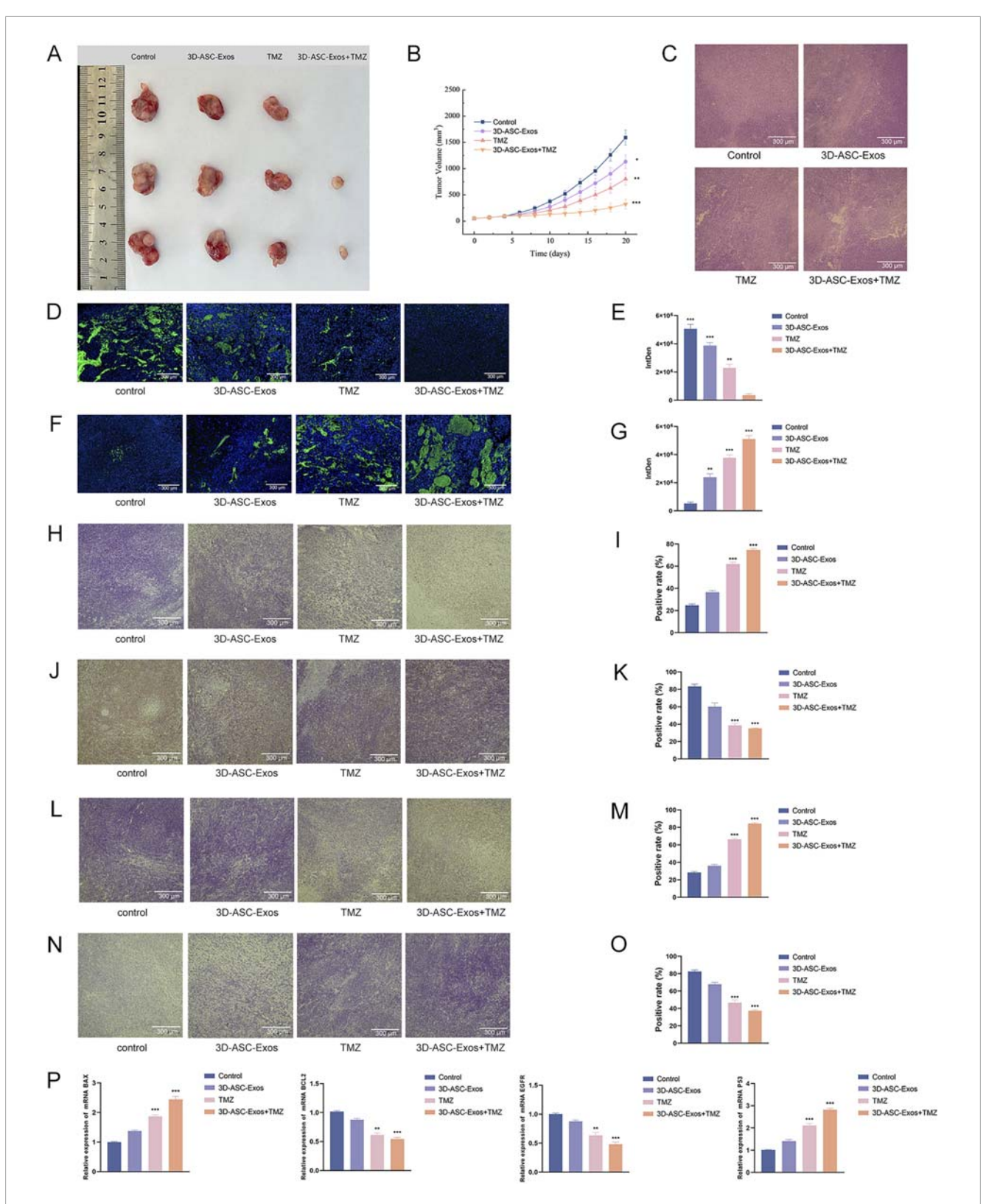


FIGURE 7 Evaluation of the anti-glioma efficacy of 3D-ASC-Exos loaded with TMZ. (A) Gross observation of tumors. (B) Trend of tumor volume changes. (C) HE staining of tumor tissues (n = 3). (D) Ki67 fluorescence staining of tumors. (E) Quantitative analysis of Ki67 staining (n = 3). (F) TUNEL staining of tumors. (G) Quantitative analysis of TUNEL staining (n = 3). (H) Immunohistochemical detection of BAX expression in tumor tissues. (I) Quantitative analysis of BCL2 (n = 3). (L) Immunohistochemical detection of BCL2 expression in tumor tissues. (K) Quantitative analysis of BCL2 (n = 3). (L) Immunohistochemical detection of P53 expression in tumor tissues. (M) Quantitative analysis of P53 (n = 3). (N) Immunohistochemical detection of EGFR expression in tumor tissues. (O) Quantitative analysis of EGFR (n = 3). (P) Q-PCR analysis of the expression levels of BAX, BCL2, P53, and EGFR (n = 3). The relative gene expression levels were calculated using the $2^{-\Delta\Delta Ct}$ method. Data were presented as mean \pm SD. One-way ANOVA combined with Tukey's HSD test and Bonferroni correction was used. "P < 0.05, **P < 0.01, ***P < 0.001.

of this nude mouse had been cured. The surfaces of the grayishwhite tumors of the other two mice also showed almost no blood vessels, indicating that the tumor development process of these two nude mice was significantly inhibited. The HE staining results of the tumor tissues showed that in the 3D-ASC-Exos + TMZ group, the surface fissures of the slices spread from the center to every part of the tumor, and dense fissures and vacuoles appeared inside the tumor. Even the deep-stained areas were no longer full (Figure 7C). The above results indicated that the tumor had begun to disintegrate internally. The Ki67 fluorescence staining results of tumor sections showed that in the 3D-ASC-Exos + TMZ group, the positive staining area almost disappeared, with only a few scattered positive staining spots remaining (Figures 7D,E). The result indicated that the tumor's proliferative capacity had almost vanished at this time. The total fluorescence intensity of the positive area in each group was used as the quantitative value. The TUNEL staining results indicated that in the 3D-ASC-Exos + TMZ group, the positive areas had occupied the entire section, and the positive cells were connected together, suggesting that severe apoptosis had occurred in the tumor tissue at this time, and the degree of apoptosis was more severe compared to the TMZ group (Figures 7F,G). The immunohistochemistry and Q-PCR results indicated that 3D-ASC-Exos loaded with TMZ significantly downregulated the expression of the oncogenes BCL2 and EGFR, and promoted the expression of the tumor suppressor genes P53 and BAX (Figures 7H-P). The above results suggested that 3D-ASC-Exos loaded with TMZ could effectively inhibit the development process of glioma. In conclusion, 3D-ASC-Exos had shown excellent anti-cancer effects as drug delivery carriers and had mitigated the adverse effects on the body caused by the intake of pure drugs. It was worth noting that in this study, since the tumor-bearing mice were subjected to ectopic modeling, there might be differences compared to the actual therapeutic effects of glioma.

4 Conclusion

This study established a 3D hollow fiber bioreactor system for ASCs culture. The total amount and concentration of exosomes obtained by this method were 10 times and 30 times those obtained by the 2D method, respectively. 3D-ASC-Exos had the same morphology and properties as 2D-ASC-Exos. However, 3D-ASC-Exos were enriched with more miRNAs related to tumor suppression. Due to the subcutaneous inoculation modeling method lacking a complete blood-brain barrier structure, drugs could directly contact tumor cells. Therefore, this manuscript was more suitable for evaluating the direct anti-tumor effect of drugs, and at the same time, it could more truly reflect the systemic toxicity and metabolic characteristics of the drugs. In future research, we will conduct more in-depth studies on whether 3D-ASC-Exos carrying TMZ can penetrate the blood-brain barrier. Both in vitro and in vivo studies had shown that 3D-ASC-Exos loaded with TMZ could inhibit the proliferation, migration and invasion of glioma cells and promote apoptosis, thereby exerting anti-glioma effects. Meanwhile, 3D-ASC-Exos had excellent systemic safety and biocompatibility, which could reduce the damage of chemotherapy drugs to the body. The development of 3D-ASC-Exos as a drug delivery carrier not only offers a superior tumor treatment strategy but also demonstrates the broad potential of exosomes in targeted tumor therapy.

Data availability statement

The datasets presented in this study can be found in online repositories. The names of the repository/repositories and accession number(s) can be found in the article/Supplementary Material.

Ethics statement

The animal study was approved by All experimental procedures involving animals were conducted in accordance with the ethical policies and guidelines approved by the Animal Ethics Committee of Jilin Agricultural University. The study was conducted in accordance with the local legislation and institutional requirements.

Author contributions

XH: Methodology, Data curation, Writing – original draft. XL: Validation, Methodology, Writing – original draft. XY: Validation, Writing – original draft. YZ: Writing – original draft, Validation. CL: Methodology, Writing – original draft. WL: Writing – original draft, Visualization. RH: Writing – original draft, Software. YL: Validation, Writing – original draft. JL: Writing – review and editing, Project administration. ND: Project administration, Writing – review and editing. BJ: Supervision, Project administration, Writing – review and editing, Writing – original draft. RD: Supervision, Writing – review and editing.

Funding

The author(s) declare that financial support was received for the research and/or publication of this article. This study was funded by Jilin Provincial Key Research and Development Plan Project (Grant/Award Number: 20240305088YY).

Conflict of interest

The authors declare that the research was conducted in the absence of any commercial or financial relationships that could be construed as a potential conflict of interest.

Generative AI statement

The author(s) declare that no Generative AI was used in the creation of this manuscript.

Any alternative text (alt text) provided alongside figures in this article has been generated by Frontiers with the support of artificial intelligence and reasonable efforts have

been made to ensure accuracy, including review by the authors wherever possible. If you identify any issues, please contact us.

reviewers. Any product that may be evaluated in this article, or claim that may be made by its manufacturer, is not guaranteed or endorsed by the publisher.

Publisher's note

All claims expressed in this article are solely those of the authors and do not necessarily represent those of their affiliated organizations, or those of the publisher, the editors and the

Supplementary material

The Supplementary Material for this article can be found online at: https://www.frontiersin.org/articles/10.3389/fcell.2025.1677555/full#supplementary-material

References

Bagheri, E., Abnous, K., Farzad, S. A., Taghdisi, S. M., Ramezani, M., and Alibolandi, M. (2020). Targeted doxorubicin-loaded mesenchymal stem cells-derived exosomes as a versatile platform for fighting against colorectal cancer. *Life Sci.* 261, 118369. doi:10.1016/j.lfs.2020.118369

Bushnell, G. G., Sharma, D., Wilmot, H. C., Zheng, M., Fashina, T. D., Hutchens, C. M., et al. (2024). Natural killer cell regulation of breast cancer stem cells mediates metastatic dormancy. *Cancer Res.* 84 (20), 3337–3353. doi:10.1158/0008-5472.CAN-24-0030

Cao, J., Wang, B., Tang, T., Lv, L., Ding, Z., Li, Z., et al. (2020). Three-dimensional culture of MSCs produces exosomes with improved yield and enhanced therapeutic efficacy for cisplatin-induced acute kidney injury. Stem Cell Res. Ther. 11 (1), 206. doi:10.1186/s13287-020-01719-2

Chen, X., Lin, Q., Jiang, Y., Wang, C., Min, F., Ou, Y., et al. (2022). Identification of potential biomarkers of platelet RNA in glioblastoma by bioinformatics analysis. *BioMed Res. Int.* 2022, 2488139. doi:10.1155/2022/2488139

Chonco, L., Landete-Castillejos, T., Serrano-Heras, G., Serrano, M. P., Pérez-Barbería, F. J., González-Armesto, C., et al. (2021). Anti-tumour activity of deer growing antlers and its potential applications in the treatment of malignant gliomas. *Sci. Rep.* 11 (1), 42. doi:10.1038/s41598-020-79779-w

de Miguel, F. J., Gentile, C., Feng, W. W., Silva, S. J., Sankar, A., Exposito, F., et al. (2023). Mammalian SWI/SNF chromatin remodeling complexes promote tyrosine kinase inhibitor resistance in EGFR-Mutant lung cancer. *Cancer Cell* 41 (8), 1516–1534.e9. doi:10.1016/j.ccell.2023.07.005

Dominici, M., Le Blanc, K., Mueller, I., Slaper-Cortenbach, I., Marini, F., Krause, D., et al. (2006). Minimal criteria for defining multipotent mesenchymal stromal cells. The international society for cellular therapy position statement. *Cytotherapy* 8 (4), 315–317. doi:10.1080/14653240600855905

Fernandes, C., Costa, A., Osório, L., Lago, R. C., Linhares, P., Carvalho, B., et al. (2017). Current standards of care in glioblastoma therapy. In: S. De Vleeschouwer, editor. *Glioblastoma*. Brisbane, AU: Codon Publications.

Gobin, J., Muradia, G., Mehic, J., Westwood, C., Couvrette, L., Stalker, A., et al. (2021). Hollow-fiber bioreactor production of extracellular vesicles from human bone marrow mesenchymal stromal cells yields nanovesicles that mirrors the immuno-modulatory antigenic signature of the producer cell. *Stem cell Res. and Ther.* 12 (1), 127. doi:10.1186/s13287-021-02190-3

Guo, Q., Yan, J., Song, T., Zhong, C., Kuang, J., Mo, Y., et al. (2020). microRNA-130b-3p contained in MSC-derived EVs promotes lung cancer progression by regulating the FOXO3/NFE2L2/TXNRD1 axis. *Mol. Ther. Oncolytics* 20, 132–146. doi:10.1016/j.omto.2020.09.005

Hu, D., Li, X., Nie, S., and Wang, S. (2022). Role of biomimetic nanomaterials made from glioma cell-derived extracellular vesicles in targeted delivery of STAT3-siRNA. *Med. Sci.* 47 (12), 1646–1654. doi:10.11817/j.issn.1672-7347.2022.210764

Jezierzański, M., Nafalska, N., Stopyra, M., Furgoł, T., Miciak, M., Kabut, J., et al. (2024). Temozolomide (TMZ) in the treatment of glioblastoma Multiforme-A literature review and clinical outcomes. *Curr. Oncol.* 31 (7), 3994–4002. doi:10.3390/curroncol31070296

Jia, B., Zhang, L., Zhang, Y., Ge, C., Yang, F., Du, R., et al. (2021). Integrated analysis of miRNA and mRNA transcriptomic reveals antler growth regulatory network. *Mol. Genet. Genom* 296 (3), 689–703. doi:10.1007/s00438-021-01776-z

Kizhakkeppurath Kumaran, A., Sahu, A., Singh, A., Aynikkattil Ravindran, N., Sekhar Chatterjee, N., Mathew, S., et al. (2023). Proteoglycans in breast cancer, identification and characterization by LC-MS/MS assisted proteomics approach: a review. *Proteomics. Clin. Appl.* 17 (4), e2200046. doi:10.1002/prca. 202200046

Li, C., Li, Y., Wang, W., Scimeca, M., Melino, G., Du, R., et al. (2023). Deer antlers: the fastest growing tissue with least cancer occurrence. *Cell Death Differ.* 30 (12), 2452–2461. doi:10.1038/s41418-023-01231-z

Liang, L., Zhao, L., Wang, Y., and Wang, Y. (2021). Treatment for hepatocellular carcinoma is enhanced when norcantharidin is encapsulated in exosomes derived from bone marrow mesenchymal stem cells. *Mol. Pharm.* 18 (3), 1003–1013. doi:10.1021/acs.molpharmaceut.0c00976

Liu, X., Xie, P., Hao, N., Zhang, M., Liu, Y., Liu, P., et al. (2021). HIF-1-regulated expression of calreticulin promotes breast tumorigenesis and progression through Wnt/β-catenin pathway activation. *Proc. Natl. Acad. Sci. U. S. A.* 118 (44), e2109144118. doi:10.1073/pnas.2109144118

Liu, L., Jiao, Y., Yang, M., Wu, L., Long, G., and Hu, W. (2023). Network pharmacology, molecular docking and molecular dynamics to explore the potential immunomodulatory mechanisms of deer antler. *Int. J. Mol. Sci.* 24 (12), 10370. doi:10.3390/ijms241210370

Lv, X., Niu, W., Zhang, B., Chen, J., Yang, S., Xue, Y., et al. (2024). Self-assembled peptide hydrogels loaded with umbilical cord-derived mesenchymal stem cells repairing injured endometrium and restoring fertility. *Adv. Healthc. Mater.* 13 (32), e2400524. doi:10.1002/adhm.202400524

Mithoowani, H., and Febbraro, M. (2022). Non-small-cell lung cancer in 2022: a review for general practitioners in oncology. *Curr. Oncol.* 29 (3), 1828–1839. doi:10.3390/curroncol29030150

Moyer, A., Tanaka, K., and Cheng, E. H. (2025). Apoptosis in cancer biology and therapy. *Annu. Rev. Pathol.* 20 (1), 303–328. doi:10.1146/annurev-pathmechdis-051222-115023

Nieto-Diaz, M., Pita-Thomas, D. W., Munoz-Galdeano, T., Martinez-Maza, C., Navarro-Ruiz, R., Reigada, D., et al. (2012). Deer antler innervation and regeneration. Front. Biosci. 17 (4), 1389–1401. doi:10.2741/3993

Ogawa, D., Ansari, K., Nowicki, M. O., Salińska, E., Bronisz, A., and Godlewski, J. (2019). MicroRNA-451 inhibits migration of glioblastoma while making it more susceptible to conventional therapy. *Non-coding RNA* 5 (1), 25. doi:10.3390/ncrna5010025

Phan, J., Kumar, P., Hao, D., Gao, K., Farmer, D., and Wang, A. (2018). Engineering mesenchymal stem cells to improve their exosome efficacy and yield for cell-free therapy. *J. Extracell. Vesicles* 7 (1), 1522236. doi:10.1080/20013078.2018.1522236

Ren, W., Hou, J., Yang, C., Wang, H., Wu, S., Wu, Y., et al. (2019). Extracellular vesicles secreted by hypoxia pre-challenged mesenchymal stem cells promote non-small cell lung cancer cell growth and mobility as well as macrophage M2 polarization via miR-21-5p delivery. *J. Exp. and Clin. Cancer Res.* 38 (1), 62. doi:10.1186/s13046-019-1027-0

Safari, F., Ansari Dogaheh, F., and Dadashi, H. (2023). Evaluation of SgK269 expression in Colon cancer patients and the effects of hAMSCs secretome on tumor invasion through SgK269/c-Src/p-P130Cas/p-Paxillin/p-ERK1/2 signaling pathway in HT-29 Colon cancer cells. *3 Biotech.* 13 (11), 346. doi:10.1007/s13205-023-03763-0

Shi, S., Zhang, Q., Xia, Y., You, B., Shan, Y., Bao, L., et al. (2016). Mesenchymal stem cell-derived exosomes facilitate nasopharyngeal carcinoma progression. *Am. J. cancer Res.* 6 (2), 459–472.

Storm, M. P., Sorrell, I., Shipley, R., Regan, S., Luetchford, K. A., Sathish, J., et al. (2016). Hollow Fiber bioreactors for in vivo-like mammalian tissue culture. *J. Vis. Exp.* (111), 53431. doi:10.3791/53431

Ueyama, H., Okano, T., Orita, K., Mamoto, K., Yamada, Y., and Nakamura, H. (2023). Three-dimensional adipose-derived stem cell spheroids exert potent therapeutic effects on rat femur osteochondral defects. *Knee* 42, 382–389. doi:10.1016/j.knee. 2023.04.017

van Niel, G., Carter, D. R. F., Clayton, A., Lambert, D. W., Raposo, G., and Vader, P. (2022). Challenges and directions in studying cell-cell communication by extracellular vesicles. *Nat. Rev. Mol. Cell Biol.* 23 (5), 369–382. doi:10.1038/s41580-022-00460-3

Watson, D. C., Bayik, D., Srivatsan, A., Bergamaschi, C., Valentin, A., Niu, G., et al. (2016). Efficient production and enhanced tumor delivery of engineered extracellular vesicles. *Biomaterials* 105, 195–205. doi:10.1016/j.biomaterials.2016.07.003

Wei, H., Chen, J., Wang, S., Fu, F., Zhu, X., Wu, C., et al. (2019). A nanodrug consisting of doxorubicin and exosome derived from mesenchymal stem cells for osteosarcoma treatment *in vitro*. *Int. J. Nanomed.* 14, 8603–8610. doi:10.2147/IJN.S218988

- Wu, S., Ju, G. Q., Du, T., Zhu, Y. J., and Liu, G. H. (2013). Microvesicles derived from human umbilical cord Wharton's jelly mesenchymal stem cells attenuate bladder tumor cell growth *in vitro* and *in vivo*. *PloS One* 8 (4), e61366. doi:10.1371/journal.pone.0061366
- Wu, J., Li, S., Wang, H., Qi, Y., Tao, S., Tang, P., et al. (2025). High-yield BMSC-Derived exosomes by the 3D culture system to enhance the skin wound repair. *Regen. Biomater.* 12, rbaf022. doi:10.1093/rb/rbaf022
- Yan, I. K., Shukla, N., Borrelli, D. A., and Patel, T. (2018). Use of a hollow fiber bioreactor to collect extracellular vesicles from cells in culture. *Methods Mol. Biol.* 1740, 35–41. doi:10.1007/978-1-4939-7652-2_4
- Zhang, X., Yang, Y., Yang, Y., Chen, H., Tu, H., and Li, J. (2020). Exosomes from bone marrow microenvironment-derived mesenchymal stem cells affect CML cells growth

and promote drug resistance to tyrosine kinase inhibitors. Stem Cells Int. 2020, 8890201. doi: 10.1155/2020/8890201

Zhao, K., Wang, L., Li, T., Zhu, M., Zhang, C., Chen, L., et al. (2017). The role of miR-451 in the switching between proliferation and migration in malignant glioma cells: AMPK signaling, mTOR modulation and Rac1 activation required. *Int. J. Oncol.* 50 (6), 1989–1999. doi:10.3892/ijo. 2017.3973

Zhao, W., Qin, P., Zhang, D., Cui, X., Gao, J., Yu, Z., et al. (2019). Long non-coding RNA PVT1 encapsulated in bone marrow mesenchymal stem cell-derived exosomes promotes osteosarcoma growth and metastasis by stabilizing ERG and sponging miR-183-5p. *Aging* 11 (21), 9581–9596. doi:10.18632/aging.102406

Zhou, Y., Yu, S., and Zhang, W. (2023). NOD-Like receptor signaling pathway in gastrointestinal inflammatory diseases and cancers. *Int. J. Mol. Sci.* 24 (19), 14511. doi:10.3390/ijms241914511